Struct Chem (2016) 27:1265–1278
DOI 10.1007/s11224-016-0755-4

ORIGINAL RESEARCH

The nitrogen inversion in fused isoxazolidinyl derivatives of substituted uracil: synthesis, NMR and computational analysis

Mateusz Kuprianowicz[1] · Marcin Kaźmierczak[1] · Hanna Wójtowicz-Rajchel[1]

Received: 14 January 2016 / Accepted: 22 March 2016 / Published online: 8 April 2016

Abstract A series of fused isoxazolidines have been prepared via 1,3-dipolar cycloaddition reactions of *N*-protected methylenenitrones with 1,3-dimethyluracil derivatives, and their NMR spectra have been recorded in TFA-*d* and in $CDCl_3$ over a wide range of temperatures. The spectra indicate the presence of two invertomers for all isoxazolidines. Barriers to nitrogen inversion in the cycloadduct **6a** have been determined using DFT quantochemical calculations. Our estimates have shown that the inversion proceeds at more complex path, involving four structures of local minima and four transition states.

Keywords Nitrogen inversion · Isoxazolidines · Quantum chemical calculations · NMR spectroscopy

Introduction

A number of nucleosides, nucleotides and nucleic acid bases with modified pyrimidine moieties are currently undergoing evaluation as antiviral agents and modifications primarily at the 5- and/or 6-position of the pyrimidine base have been extensively studied [1]. Part of this effort has involved the utilization of the C^5=C^6 double bond for synthetic elaboration by means of nucleophilic and electrophilic reactions [2] or cycloaddition processes. Although the intermolecular cycloaddition reaction is one of the most versatile tools for the synthesis of fused heterocyclic systems [3–5], only a few examples of their application to the modification of uridine and uracil derivatives are reported in the literature. Keana et al. [6] described the preparation of the key intermediate for *tetrodotoxin* derivative in the Diels–Alder reaction of butadiene with appropriately functionalized orotates. Saladino et al. [7] reported the reaction of lithium trimethylsilyldiazomethane and diazomethane with uracil. Pellissier et al. [8] investigated the cobalt-mediated [2.2.2] cycloaddition of pyrimidine derivatives to alkynes, and Negron and coworkers obtained bicyclic *N*-methylpyrrolidine thymidine derivatives using cycloaddition reaction of azomethine ylide with bis-*O*-silylthymidines [9]. Finally, Colacino and coworkers obtained in reaction between nitrone and 1-*N*-vinyluracil a new isoxazolidine derivative fused with the pyrimidine moiety, as a competitive product to 4′-aza-analogues of 2′,3′-dideoxynucleotides [10].

Nitrones are valuable synthons in the organic synthesis which are extensively used in the synthesis of biologically active compounds [11, 12], as spin trap reagents [13], as therapeutic agents [14, 15] and primarily behave like 1,3-dipoles in cycloaddition reactions giving isoxazolidines [16]. Isoxazolidines are already well established as heterocyclic analogues of the five-membered sugar moiety of nucleosides, and a variety of isoxazolidine-based molecules are being tested for antiviral and anticancer activities [17].

The 1,3-dipolar cycloaddition of the nitrone dipole to the double bond provides a convenient entry into the isoxazolidine ring system having an N–O moiety embedded in the ring skeleton. Generally, it takes place in a regioselective and stereocontrolled manner, because the cycloaddition reaction conserves the stereochemistry of the

Electronic supplementary material The online version of this article (doi:10.1007/s11224-016-0755-4) contains supplementary material, which is available to authorized users.

✉ Hanna Wójtowicz-Rajchel
wojto@amu.edu.pl

[1] Faculty of Chemistry, Adam Mickiewicz University, Umultowska 89b., 61-614 Poznań, Poland

alkene. However, the conformational aspect is not so obvious and the conformation of very flexible five-membered ring is not well defined [18]. Moreover, it has been shown that unshared orbital interactions on neighboring heteroatoms such as those present in isoxazolidines are responsible for a considerable energy barrier toward ring inversion [19]. Oxygen being next to nitrogen raises the barrier to nitrogen inversion to such an extent that the individual invertomers can be identified by NMR spectroscopy [20, 21].

Experimental

General information

N-Cyclohexylhydroxylamine [22], 5-chlorouracil [23], 1,3-dimethy-5-nitrouracil [24] and 1,3-dimethyl derivatives of uracils **2**, **3** and **5** were prepared according to the literature [25]. All other starting materials and reagents were obtained from Sigma-Aldrich. Toluene was distilled from NaH and was stored over molecular sieves (0.4 nm). All reactions were monitored by TLC. Thin-layer chromatography was performed with 60 F_{254} TLC plates (Merck). Column chromatography was performed with silica gel (Merck, particle size 0.063–0.200 mm, 70–230 mesh). The cycloaddition reactions were carried out in glass pressure tubes equipped with a magnetic stirrer.

^{1}H NMR, ^{13}C NMR and ^{19}F NMR spectra were performed on Varian GEMINI 300 (300 MHz), Varian 400 (400 MHz), Bruker Avance 400 (400 MHz) and Bruker Avance 600 (600 MHz) spectrometers. Temperature control was achieved using a Bruker cooling unit (BCU-II) to provide chilled air. The experiments were performed without sample spinning. Chemical shifts of ^{1}H NMR were expressed in parts per million downfield from tetramethylsilane (TMS) as an internal standard ($\delta = 0$) in $CDCl_3$. Chemical shifts of ^{13}C NMR were expressed in parts per million downfield from $CDCl_3$ as an internal standard ($\delta = 77.0$). Chemical shifts of ^{19}F NMR were expressed in parts per million upfield from $CFCl_3$ as an internal standard ($\delta = 0$) in $CDCl_3$.

The mass spectra were recorded on a 320MS/450GC Bruker and AMD 402 spectrometer, and ionization was achieved through electron impact (EI). High-resolution data were obtained on the same instrument using a peak-matching technique. Elemental composition of the discussed ion was determined with an error of less than 10 ppm in relation to perfluorokerosene at resolving power of 10000. The elemental analyses were made on Vario EL III Element Analyzer.

All computations in this study including DFT NMR calculations were performed by Gaussian 09 program package [26]. The DFT geometry optimizations have been performed using different functional, namely B3LYP [27], WB97XD [28], M06 [29] with 6–31G(*d*) and 6–31++G(*d*,*p*). Geometry optimizations were confirmed by the vibrational frequency calculations at each level. In DFT NMR calculations, the geometry optimizations were calculated using the B3LYP method on 6–31G(*d*), 6–31G(*d*,*p*), 6–31++G(*d*,*p*), 6–31G(2*d*,2*p*) and 6–31++G(2*d*,2*p*) level of theory. Solution-state calculations used default and IEFPCM [30] model, as implemented in Gaussian 09. ^{13}C NMR chemical shifts were computed at the B3LYP/6–31G(*d*), 6–31G(*d*,*p*), 6–31++G(*d*,*p*), 6–31G(2*d*,2*p*) and 6–31++G(2*d*,2*p*) level using the GIAO method [31] and are given relative to that of TMS calculated at the same level of theory.

The quantochemical research was supported in part by PL-Grid Infrastructure.

Typical synthetic procedure

A mixture of paraformaldehyde (60 mg, 2 mmol), triethylamine (222 mg, 2.2 mmol) and *N*-methylhydroxylamine hydrochloride, *N*-*t*-butylhydroxylamine or *N*-benzylhydroxylamine hydrochloride (2 mmol) in anhydrous toluene (10–15 mL) was placed in a glass pressure tube equipped with a magnetic stirrer and stirred at 70 °C for 1 h. Only *N*-cyclohexylhydroxylamine was used as a free base. The solution was cooled to room temperature, the corresponding 1,3-dimethyluracils **2–5** (1 mmol) was then added, and the solution was heated at 60–80 °C for 24–48 h. The solvent was evaporated to dryness under reduced pressure, and 10–15 mL of water was added. The aqueous solution was extracted a few times with $CHCl_3$ and the combined extract dried over Na_2SO_4. Solvent was removed, and the crude product was separated by column chromatography (silica gel, hexane, a gradient of hexane/CH_2Cl_2, CH_2Cl_2 or a gradient of hexane/ethyl acetate) to give compounds **6a–9d**. The detailed spectral data of compounds **6a–9d** and **10a–10d** can be found in the Supporting Information, and the representative analytical data of compound **6a** are given below.

Analytical data of compound 6a

Compound 6a *3a-Fluoro-2,5,7-trimethyltetrahydroisoxazolo[5,4-d]pyrimidine-4,6(2H,5H)-dione*

Oil, 78 % yield. Room temperature NMR: ^{1}H NMR (300 MHz, $CDCl_3$) δ 5.18 (d, $J = 18.3$ Hz, 1 H, C^{6}–H), 4.00–3.20 (vbs, 2 H, CH_2), 3.17 (bs, 3 H, N-CH_3), 3.00 (bs, 3 H, N–CH_3), 2.71 (bs, 3 H, N–CH_3). ^{19}F NMR (282 MHz, $CDCl_3$) δ −159.06 (bs), −159.77 (bs). TFA NMR: ^{1}H

NMR (400 MHz, TFA-*d*) Major invertomer: δ 6.08 (d, $J = 11.7$ Hz, 1 H, C^6–H), 5.24 (dd, $J = 13.8$, 28.9 Hz, 1 H, C^9–H^a), 4.46 (dd, $J = 13.8$, 21.9 Hz, 1H, C^9–H^b), 3.69 (s, 3 H, N-CH_3), 3.40 (s, 3 H, N–CH_3), 3.23 (s, 3 H, N–CH_3). Minor invertomer: δ 6.15 (d, $J = 14.3$ Hz, 1 H, C^6–H), 5.23 (m, 1 H, C^9–H^a), 4.46 (dd, $J = 13.6$, 27.1 Hz, 1 H, C^9–H^b), 3.67 (s, 3 H, N–CH_3), 3.43 (s, 3 H, N–CH_3), 3.32 (s, 3 H, N–CH_3). Low-temperature NMR: ^{1}H NMR (600 MHz, $CDCl_3$) Major invertomer: δ 5.23 (d, $J = 17.8$ Hz, 1 H, C^6–H), 3.70 (t, $J = 9.9$ Hz, 1 H, C^9–H^a), 3.05 (dd, $J = 10.6$, 24.9 Hz, 1 H, C^9–H^b), 3.18 (s, 3 H, N–CH_3), 2.99 (s, 3 H, N–CH_3, 2.74 (s, 3H, N–CH_3). Minor invertomer: δ 5.16 (d, $J = 19.6$ Hz, 1 H, C^6–H), 3.83 (dd, $J = 12.5$, 20.6 Hz, 1 H, C^9–H^a), 2.78 (dd, $J = 12.5$, 27.8 Hz, 1 H, C^9–H^b), 3.78 (s, 3 H, N–CH_3), 3.18 (s, 3 H, N–CH_3), 2.71 (s, 3 H, N–CH_3). ^{19}F NMR (565 MHz, $CDCl_3$) δ −159.71 (m), −158.93 (m). ^{13}C NMR (151 MHz, $CDCl_3$) Major invertomer: δ 165.40 (d, $J = 26.4$ Hz), 150.56, 97.12 (d, $J = 193.4$ Hz), 88.45 (d, $J = 32.8$ Hz), 67.80 (d, $J = 28.2$ Hz), 44.49, 32.44, 28.59. Minor invertomer: δ 164.79 (d, $J = 26.4$ Hz), 150.20, 95.70 (d, $J = 195.4$ Hz), 88.76 (d, $J = 35.2$ Hz), 67.14 (d, $J = 25.6$ Hz), 44.87, 34.75, 28.40. MS (EI, %) m/z 217 (M^+, 13 %). HRMS (EI) calcd for $C_8H_{12}FN_3O_3$: 217.08627, found: 217.08503. Elemental analysis. Found: C, 44.12; H, 5.73; N, 19.11. Calc. for $C_8H_{12}FN_3O_3$ (217.20): C, 44.24; H, 5.57; N, 19.35 %.

Results and discussion

In the course of our work on fluorovinyl derivatives of nucleic acid bases and their cycloaddition reactions with nitrones [32–34], we decided to synthesize a series of isoxazolidinyl derivatives of 5-fluorouracil in 1,3-dipolar cycloaddition of *N*-fluorovinyl-5-fluorouracil with nitrones. Unexpectedly, we obtained exclusively, without any competitive reaction, the cycloaddition product not to exocyclic, but to endocyclic double bond with the formation of fused ring. To our knowledge, there was only one report that deals with the reaction of pyrimidines with nitrones [10]. In continuation of our recent studies, we decided to apply the nitrone–olefin cycloaddition to the formation of fused isoxazolidines in reactions of methylenenitrones with 5-substituted 1,3-dimethyluracils, to evaluate the reaction regioselectivity and the conformation/configuration of the resultant cycloadducts. Thus, condensation reaction of *N*-alkyl hydroxylamines with formaldehyde followed by in situ 1,3-dipolar cyclization of the resulting achiral nitrones with pyrimidinic nucleophiles affords compounds **6a–6d**, **7a–7d**, **8a–8d**, **9a** and **9d** (Scheme 1). The obtained fused isoxazolidines showed spectral properties that are

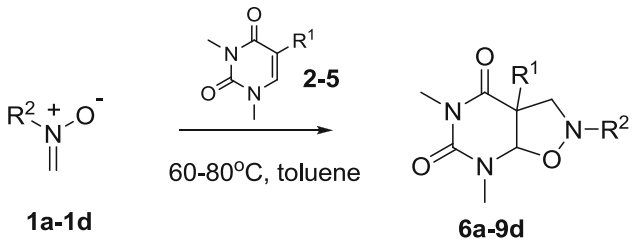

Scheme 1 Synthetic scheme for isoxazolidinyl derivatives **6a–9d**

typical for systems exhibiting slow inversion on the nitrogen atom—a significant broadening of signals in the spectra of proton and carbon NMR. They represent the additional examples of molecules which can exhibit chemical shift nonequivalence due to hindered stereomutation at nitrogen [35–37].

The cycloaddition took place with complete regioselectivity and with stereospecific generation of two consecutive stereocenters. The theoretical studies have indicated that 1,3-dipolar cycloaddition reactions proceed through a concerted mechanism [38], and therefore, we only considered the one step mechanism for the 1,3-dipolar cycloaddition reaction of nitrone–uracil. Indeed, cycloaddition led to products with the *cis* ring junction stereochemistry what was deduced by the coupling constant values in ^{1}H NMR spectra between newly formed ring juncture atoms in compounds **6a–6d** and **7a–7d**. Since nitrones **1a–1d** are achiral, the obtained isoxazolidines differ only in the configuration of C^5 and C^6 carbon atoms, and thus, obtained [4.3.0] bicyclic systems have two chiral centers which give indistinguishable pair of enantiomers. The regioselectivity of cycloaddition reaction results from the structure of the uracil moiety. Carbon atoms C^2, C^4 and C^6 in pyrimidine ring are characterized with diminished electron density in relation to carbon atom C^5 [39]. Uracil exhibits a comparable to pyrimidine electron density; however, electron density at C^5 atom is additionally increased by conjugation of π electrons with electrons of oxygen atom [40]. The electron density distribution in the uracil ring reflects nucleophilic and electrophilic properties of the double bond in uracils and the regioselective process of the cycloaddition. No other isomers were observed in the reaction mixtures.

However, the *N*-substituted isoxazolidinyl ring fused with almost planar six-membered ring may exhibit a special type of isomerism found in compounds with a substituent on a bridged ring system—isomerism *endo* and *exo*. The environment of the *N*-alkyl group in two isomers differs considerably. In *exo* isomer the bridgehead substituent R^1 is *anti* to the nitrogen lone pair of electrons, while in *endo* it is *syn* to the lone pair of electrons (Fig. 1). A third center of symmetry associated with chirality of the

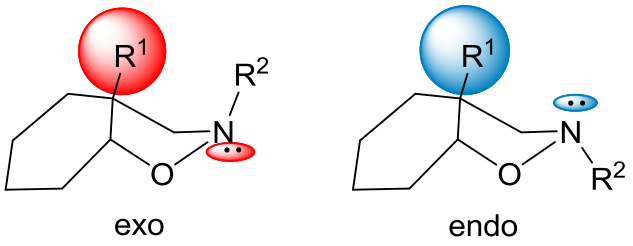

Fig. 1 *Exo* and *endo* isomerism in fused isoxazolidinyl derivatives

nitrogen atom appears, and the two diastereoisomers, under specific conditions, should be observable.

Compounds **6a–9d** gave broad ^{1}H and ^{13}C NMR signals at room temperature. This is particularly distinct for the CH_2 protons of the isoxazolidinyl ring in ^{1}H NMR spectra. In compounds **6** and **7**, the geminal protons of CH_2 group adjacent to the asymmetric carbon atom are diastereotopic and should give in ^{1}H NMR a clear AB doublets of doublets. The broadening is a result of a dynamic equilibrium between the two diastereoisomers with a different configuration for the asymmetric nitrogen atom, and the rapid inversion at room temperature of conformationally labile chiral center simplifies the AB system to A2 system. Thus, the ^{1}H NMR spectra of compounds **6a–6d** which have a fluorine atom in the C^5 showed at 5.08–5.17 ppm a doublet ($J = 18$ Hz) ascribed to the C^6–H proton, very broadened signals of CH_2 group in the range of 2.90–3.70 ppm, two distinguishable singlets from N^1- and N^3-methyl groups and signals assigned to substituents on the isoxazolidinyl nitrogen atom. ^{19}F NMR spectra showed at −159.20 to −159.40 ppm a broad singlet deriving from the C^5–F. However surprisingly, for compound **5a** we observed two broad signals of fluorine atom at −159.06 and −159.77 ppm, respectively.

Very similar ^{1}H NMR spectra were observed for compounds **7a–7d** and **8a–8d** (with the exception of compounds **7a** and **8a**). For **7a–7d** proton, C^6-H appears at 5.11–5.21 ppm as a doublet coupled to C^5–H ($J =$ 7.5–8.0 Hz). The same coupling constants are also observable for C^5–H which appears at 3.55–3.60 ppm as a multiplet. Respectively, protons C^6–H for **8b–8d** appear at 5.35–5.39 ppm as a broad singlet. Geminal methylene protons of the isoxazolidinyl ring are indistinguishable and appear as a broad signal. Only ^{1}H NMR spectra of isoxazolidines **7a** and **8a** having *N*-methyl substituent in the five-membered ring were somewhat unexpected. In compound **7a**, two diastereotopic methylene protons were visible, respectively, at 3.66 and 2.90 ppm. In compound **8a**, two sets of diastereotopic protons, broad but very distinguishable at 4.57, 3.97, 3.73 and 3.08 ppm and two diastereoisomeric protons C^6–H at 5.27 and 5.48 ppm were observed.

We studied the temperature dependence of the NMR spectra of **6a–6d** and **7a–7d** series in $CDCl_3$ within the temperature range from 273 to 223 K. Unfortunately, compounds **8a–8d** were chemically unstable and were not taken into account in the temperature study. On lowering the temperature (up to 223 K), the broad spectral lines become sharper and show two distinct forms of the compounds. The rate of nitrogen atom inversion at a sufficiently low temperature is decreased so much that signals of two invertomers are observed in the ^{1}H, ^{19}F and ^{13}C NMR spectra of examined compounds. These invertomers have different configuration at the stereogenic nitrogen atom, and we assigned them to two forms—*exo* and *endo*. The two most likely configurations of the invertomers of the isoxazolidines fused with six-membered ring are shown in Fig. 1. The figure ignores completely any conformational aspect of five-membered ring (flipping of the envelope or the twisted form). In similar systems, it is assumed that the preference of the *N*-substituent for a less hindered environment is greater than that of the lone pair [35]. We suppose that we well assigned the more intense signal to the *exo* isomer where the lone pair of electrons of the nitrogen atom is in the energetically favorable *anti* orientation to substituents at bridgehead carbon atoms. This also agrees with our calculations performed on compound **6a**.

We have also made ^{1}H NMR spectra of all compounds **6–8** and additionally **9a** and **9d** in TFA-*d* to afford for **6a–6d**, **8a–8d**, **9a** and **9d** protonated diastereoisomeric pairs of invertomers. The protonation of the lone electron pair of nitrogen in amines effectively inhibits the process of inversion. Protonation on the nitrogen atom of isoxazolidinyl ring "freezes" its configuration and eliminates the possibility of moving the configurational form one to another, and what is important, it also "freezes" the existing at a given temperature invertomers at their thermodynamic equilibrium. Thus, isoxazolidines were dissolved in TFA-*d* and ^{1}H NMR spectra were recorded immediately. Protonation of compounds **6, 8**, **9** and a solvent effect lead generally to downfield shifts of all signals in the ^{1}H NMR spectra. Each time, except for the spectra of compounds **7a–7d,** two sets of signals were obtained for all protons corresponding to the two diastereomeric forms of compounds. Only isoxazolidinyl derivatives **7a–7d** were very susceptible to acid, and in TFA-*d*, they immediately underwent the process of acid-mediated N–O cleavage to furnish quantitatively N-alkylated-C^5-methylamino derivatives of barbituric acid **10a–10d** (Scheme 2). Interestingly, ^{1}H NMR spectra of **10a–10d** showed two nonequivalent geminal H^c-C-H^d protons ($J =$ 13.6–13.9 Hz), which suggests the existence of strong intramolecular hydrogen bond and formation of the pseudo six-membered ring. This is somewhat unexpected because

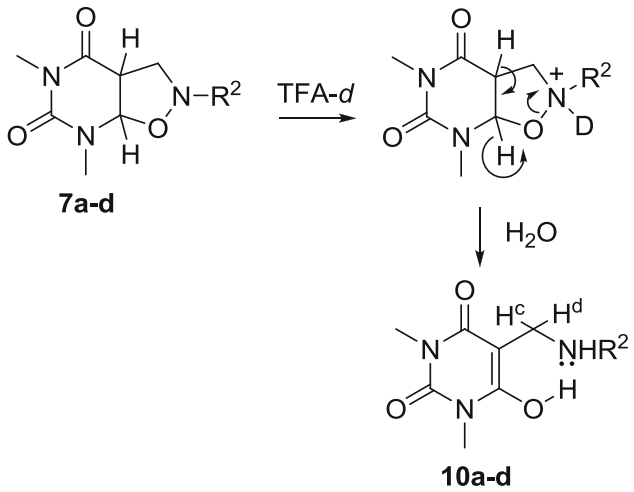

Scheme 2 Cleavage of the isoxazolidine ring in **7a**–**7d**

trifluoroacetic is a very effective hydrogen bond breaker. Moreover, the ^{1}H NMR spectra performed in $CDCl_3$, and in $CDCl_3$ after addition of D_2O, showed exactly the same pattern.

The ratios of two invertomers for compounds **6a**–**6d** and **7a**–**7d** together with experimental temperatures are shown in Table 1. Taking into account the uncertainty in determining the coalescence temperature, we gave the temperature at which well-developed signals of two diastereomers are clearly visible. Also the ratios of stereoisomeric quaternary isoxazolidines **6a**–**9d** are shown in Table 1.

Chemical shift values for protons in the isoxazolidinyl ring for diastereoisomers **6a**–**9d** are given in Table 2. In temperature experiments, the ^{1}H NMR analysis for the minor isomers is incomplete in some causes due to peak overlap. Spectra recorded in TFA-*d* gave a distinct separation of two diastereoisomeric forms.

At room temperature, all signals on the ^{1}H NMR and ^{19}F NMR and ^{13}C NMR spectra were broadened as a result of the participation of the compounds **6a**–**6d** and **7a**–**7d** in the relatively slow process of a pyramidal nitrogen inversion. To study the nature of dynamic processes, a series of variable temperature NMR experiments in range of 298–223 K were carried out. As was mentioned, the low-temperature ^{1}H, ^{19}F and ^{13}C NMR spectra of **6a**–**6d** and **7a**–**7d** show separated signals for the two invertomers. The temperature at which the spectrum reaches this state (coalescence temperature) is mostly dependent on the substituent on the isoxazolidinyl nitrogen atom.

Compounds **6a**–**6c** and **7a**–**7c** achieve very distinct separation of two invertomers in ^{1}H NMR (and ^{19}F NMR for compounds **6**) at 243 K (Fig. 2) and at temperatures somewhat higher, while compounds **6d** and **7d** having *t*-butyl substituent achieve this state until at 223 K (Fig. 3).

What is more, for the compound **6a** with the smallest alkyl substituent on the isoxazolidinyl nitrogen atom, the initial separation of signals for two invertomers is visible at 263 K and for compound **7a** already at 273 K (Fig. 4).

This is in good accord with the previous literature reports. Effects of substituents on the inversion rates of cyclic amines [41] and isoxazolidines [20, 35] have been studied by the NMR method, and it has been found that bulky groups either on the ring or on the nitrogen tend to increase the inversion rates, presumably by destabilizing the separate nonplanar configurations relative to the transition state. The bulky *t*-Bu group in sp^3-hybridized nitrogen increases the ground-state

Table 1 Preparation of isoxazolidinyl derivatives of substituted uracils

Entry	R^1	R^2	Product	Yield (%)	dr (ratio of invertomers)	
					Temperature NMR at 243 K	TFA-*d* NMR
1	F	CH_3	**6a**	78	74:26	71:29
2	F	C_6H_{11}	**6b**	69	72:28	69:32
3	F	CH_2Ph	**6c**	55	75:25	67:33
4	F	*t*-Bu	**6d**	50	84:16[a]	77:23
5	H	CH_3	**7a**	28	83:17	–[b]
6	H	C_6H_{11}	**7b**	35	79:21	–[b]
7	H	CH_2Ph	**7c**	34	76:24	–[b]
8	H	*t*-Bu	**7d**	19	81:19[a]	–[b]
9	NO_2	CH_3	**8a**	21	–	54:46
10	NO_2	C_6H_{11}	**8b**	15	–	61:39
11	NO_2	CH_2Ph	**8c**	17	–	61:39
12	NO_2	*t*-Bu	**8d**	34	–	50:40
13	Cl	CH_3	**9a**	19	–	61:39
14	Cl	*t*-Bu	**9d**	22	–	68:32

[a] Spectra recorded at 223 K

[b] Ring cleavage

Table 2 Chemical shift values of several protons of interests in isoxazolidinyl derivatives **6a-9d**

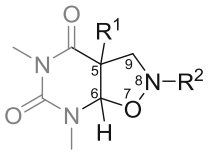

Compound	Temperature ^{1}H NMR				TFA-*d* ^{1}H NMR			
	C^5-R^1	C^6-H	N^8-R^{2a}	H^a-C^9-H^b	C^5-R^1	C^6-H	N^8-R^{2a}	H^a-C^9-H^b
6a$_{major}$	–	5.23	3.17	3.70, 3.05	–	6.08	3.69	5.24, 4.46
6a$_{minor}$	–	5.16	3.18	3.83, 2.78	–	6.15	3.67	5.23, 4.46
6b$_{major}$	–	5.18	2.65–1.00	3.71, 3.04	–	6.04	3.96–1.25	5.10, 4.58
6b$_{minor}$	–	5.15	2.40–1.00	3.88, 2.84	–	6.15	3.79–1.25	5.03, 4.50
6c$_{major}$	–	5.21	4.05, 4.01	3.67, 3.22	–	6.06	5.07, 4.97	4.98, 4.54
6c$_{minor}$	–	5.16	4.09, hidden	3.75, hidden	–	6.14	5.01, hidden	4.98, 4.52
6d$_{major}$	–	5.15	1.03	3.45, 3.17	–	6.10	1.67	4.84, 4.63
6d$_{minor}$	–	5.13	1.04	3.57, 3.17	–	6.12	1.63	4.78, 4.48
7a$_{major}$	3.67	5.25	3.20	3.67, 2.90	–	–	–	–
7a$_{minor}$	3.60	5.10	3.20	3.86, 2.89	–	–	–	–
7b$_{major}$	3.67	5.20	2.43–1.02	3.67, 2.91	–	–	–	–
7b$_{minor}$	3.59	5.08	2.43–1.02	hidden	–	–	–	–
7c$_{major}$	3.68	5.27	4.06, 3.92	3.68, 3.06	–	–	–	–
7c$_{minor}$	3.74	5.16	4.13, hidden	3.68, 3.06	–	–	–	–
7d$_{major}$	3.60	5.15	1.04	3.35, 3.15	–	–	–	–
7d$_{minor}$	3.60	5.04	1.06	3.35, 3.15	–	–	–	–
8a$_{major}$	–	–	–	–	–	6.51	3.55	5.68, 4.68
8a$_{minor}$	–	–	–	–	–	6.43	3.66	5.39, 5.11
8b$_{major}$	–	–	–	–	–	6.48	3.71–1.25	5.52, 4.83
8b$_{minor}$	–	–	–	–	–	6.44	3.93–1.25	5.32, 5.23
8c$_{major}$	–	–	–	–	–	6.47	4.87, 4.93	5.46, 4.82
8c$_{minor}$	–	–	–	–	–	6.27	5.02, 4.95	5.20, 5.20
8d$_{major}$	–	–	–	–	–	6.52	1.58	5.41, 4.94
8d$_{minor}$	–	–	–	–	–	6.46	1.66	5.30, 5.30
9a$_{major}$	–	–	–	–	–	6.18	3.48	4.96, 4.90
9a$_{minor}$	–	–	–	–	–	6.21	3.66	5.50, 4.37
9d$_{major}$	–	–	–	–	–	6.14	1.53	5.12, 4.64
9d$_{minor}$	–	–	–	–	–	6.02	1.64	5.26, 4.40

[a] For compounds **6c**, **7c** and **8c** only CH_2 protons from benzyl group are given

energy, and the sp^2-hybridized transition state, through which the nitrogen inversion occurs, has a much smaller steric congestion; hence, the activation barrier is lower than that of methyl-substituted nitrogen.

The notable conformational feature of the ^{1}H NMR spectra of obtained invertomers, both performed in TFA-*d* and at low temperatures in $CDCl_3$, is in most cases a large chemical shift anisotropy for germinal protons of isoxazolidinyl methylenes ($\Delta\delta = 0.21$–1.00 ppm for major invertomer and $\Delta\delta = 0.28$–1.13 ppm for minor invertomer). The significant differences for chemical shifts for germinal protons can be explained by considering the isoxazolidine ring geometry, it adopts the lowest energy conformation, an envelope conformation, and allowing for inversion, its nitrogen atom will either extend out from the envelope or point inside the envelope.

Only for minor invertomers of **8a–8d**, very small values of chemical shift anisotropy were observed. The $\Delta\delta$ values for **8a** are admittedly 0.28 ppm, but for **8b** $\Delta\delta$ is only 0.09 ppm. For compounds **8c** and **8d**, the anisotropy disappears entirely and the two doublets in the typical AB system go into a broad singlet. The major invertomers of **8a–8d** show $\Delta\delta$ values in the range from 0.47 to 1.00 ppm. Generally, the considerable $\Delta\delta$ values of chemical shifts

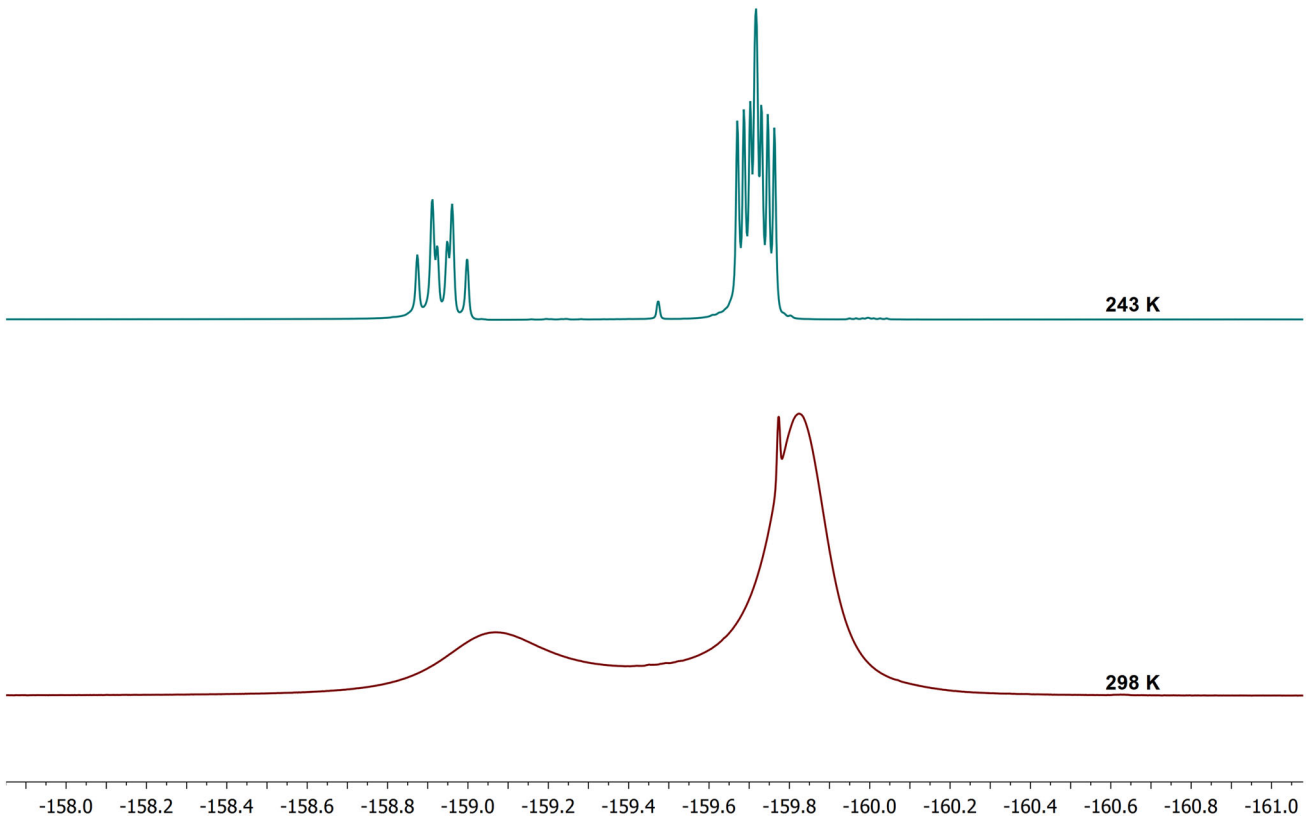

Fig. 2 The ^{19}F NMR spectra of compound **6a** in $CDCl_3$ recorded at 298 and 243 K

for isoxazolidinyl germinal protons in all the investigated compounds seem to be more dependent on isoxazolidinyl *N*-alkyls than from the C^5-substituents, and in all cases, they show the biggest value for methyl group and smallest value for *t*-butyl substituent.

To verify it, we synthesized compounds **9a** and **9d** having more abundant chlorine atom in the C^5 position, to compare them with similar **6a–8a** and **6d–8d**. Unfortunately, ^1H NMR spectra performed in TFA-*d* did not confirm fully our expectations; only for the minor invertomer the mentioned above relationship was maintained, and for major invertomer of **9a** a very small value of chemical shift anisotropy was observed. Thus, the establishment of correlation of the anisotropic effect in the tested compounds with the size of the *N*-alkyl substituent can be sometimes a small overinterpretation, although this factor is crucial, and it mainly has an effect on the slight conformational changes in the five-membered ring.

The inspection of the ^1H NMR data reveals that the geminal coupling constants of the minor invertomer in TFA-*d* are without any exception smaller than those in the dominant invertomer. Simultaneously, for compounds **6a–6d** the coupling constants (if visible) of methylene protons with vicinal fluorine C^5-F in dominant invertomer are smaller than those in the minor invertomer. Conceivably, this generality may help to determine the distinguishability of two invertomers with a different configuration for the asymmetric nitrogen atom in more complicated systems. For C^6-H protons, two separate sets of signals appear in temperature spectra in the range 5.04–5.27 ppm and in the range 6.02–6.52 in spectra performed in TFA-*d* as sharp doublets for compounds **6** and **7** (J_{HH} = 6–8 Hz, J_{HF} = 22–29 Hz) and as singlets for compounds **8** and **9**. For compounds **6c**, **7c** and **8c** having a benzyl substituent, in the ^1H NMR spectra two signals of diastereotopic benzyl protons are also observable. Two sets of two doublets in the temperature spectra appear in the range 3.99–4.03 ppm (J = 13.6–13.8 Hz) and in spectra performed in TFA-*d* in the range 4.90–5.02 ppm (J = 13.4–14.0 Hz). This is a strong evidence for the existence of "frozen" stereogenic center, adjacent to the CH_2 group.

And finally, it is also noteworthy that the nature of the *N*-substituents has little effect on the ratio between the two diastereoisomers of isoxazolidines. The exception is the value obtained for compound **7a** which is different from the pattern of the population trends in these systems, and it means the more abundant substituent, the higher ratio (see Table 1). Additionally for compounds **6a–6d**, there is a very good agreement between values obtained in the low-temperature spectra as well as in the TFA-*d* spectra. The

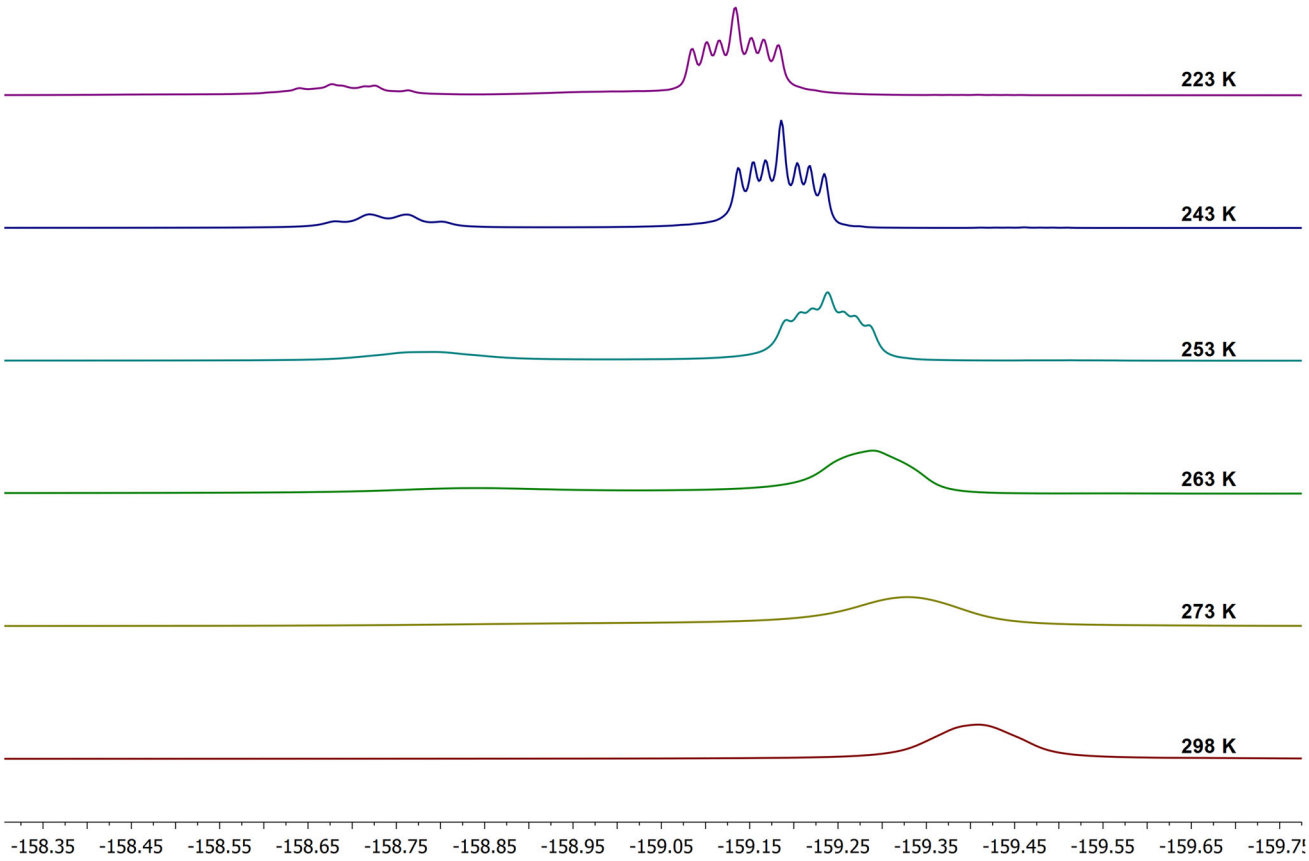

Fig. 3 The ^{19}F NMR spectra of compound **6d** in $CDCl_3$ recorded at variable temperatures

differences in the ratios of two invertomers result from different thermodynamic equilibriums in different temperatures.

Quantochemical calculations

NMR analysis at low temperatures has proven the presence of slow nitrogen inversion process. For a clear rationalization of observed results, DFT quantochemical calculations were performed to optimalize the most likely geometries of compound **6a** individual isomers and to designate the energy barrier of the observed inversion.

Preliminary geometry optimizations with B3LYP method and 6-31G(d) basis set allowed to optimize two structures differing by the nitrogen atom configuration and isoxazolidine ring conformation. In order to calculate the energy barrier of inversion between those two structures, it was necessary to find a TS structure between both minima (Scheme 3). Our research has shown that such structure probably does not exist, and the inversion proceeds at more complex path, involving additional two structures of local minima (Fig. 5) and four transition states.

In contrast to saturated six-membered rings which usually possess well-determined conformations, five-membered rings are much more flexible, so the conformation is difficult to ascertain [42]. The isoxazolidines having five-member ring system can exist in several puckered conformations with the geometry of envelope and half-chair. Ring puckering would lead to the most stable conformation of molecule which generally occurs in placing the substituents in the favorable pseudoequatorial orientation [20]. Furthermore, it has been shown that gauche relationship between the lone pairs of nitrogen and oxygen atoms is also the stabilizing factor of the whole structure [43]. The geometry optimized structures of molecule **6a** (Fig. 5) represent the group of geometries that fulfill those rules. Structures **6a–a** and **6a–b** have minimum total energy, and methyl substituent on the nitrogen atom is placed in pseudoequatorial orientation. Furthermore, in structures **6a–c** and **6a–d** methyl group is localized pseudoaxially with gauche orientation of the nitrogen and oxygen lone pairs. By placing all four structures on the potential energy surface, geometries **6a–a** and **6a–b** have the lowest total energy which could show that in our model the steric effects have the greatest impact on the most stable structure. Moreover, the structure **6a–d** has the highest total energy of all optimized minima which seems to confirm this rule. According to calculated total energies,

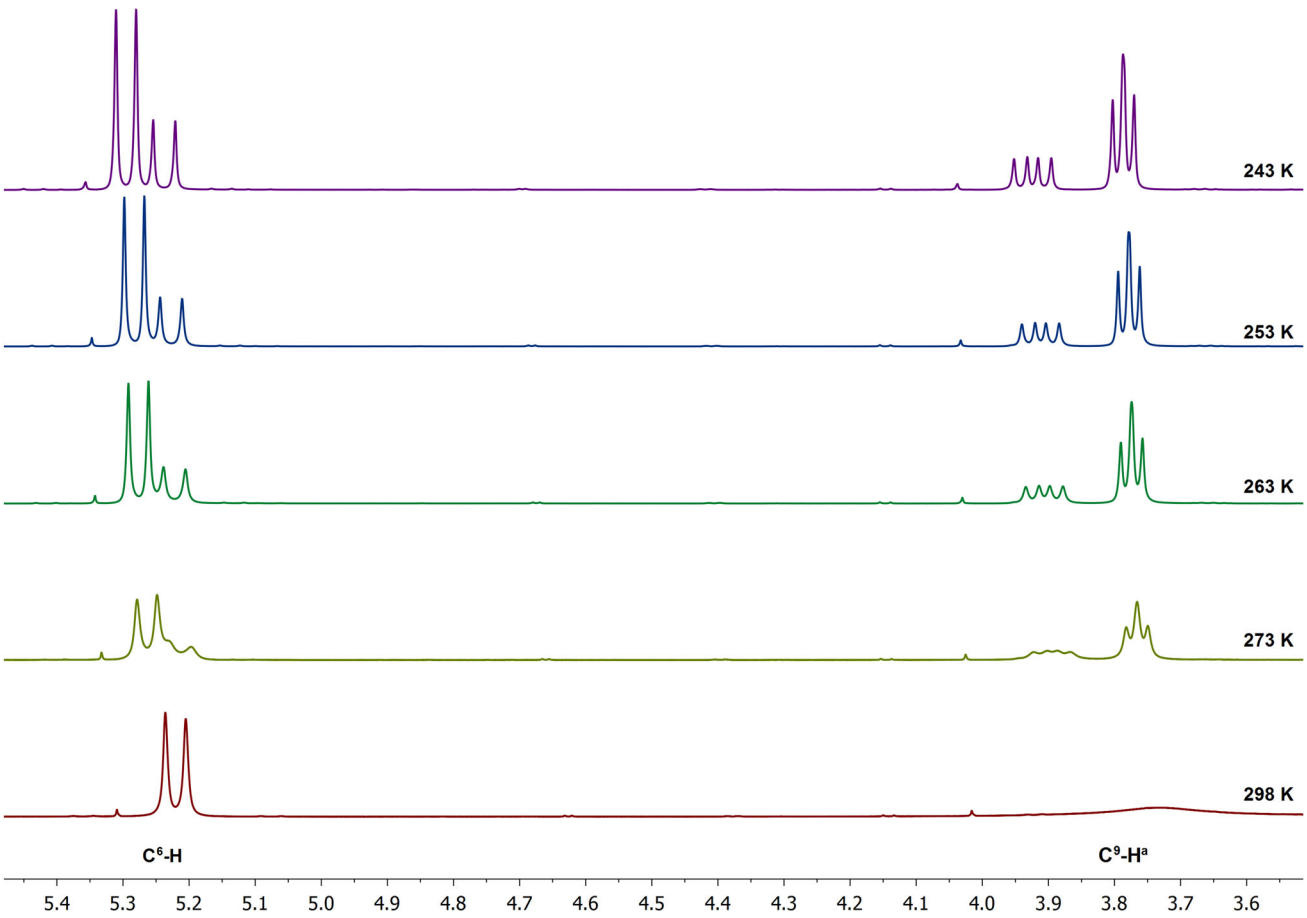

Fig. 4 The ^{1}H NMR spectra of compound **6a** in $CDCl_3$ (with the most diagnostic region of C^6–H proton and C^9–H^a proton) recorded at variable temperatures

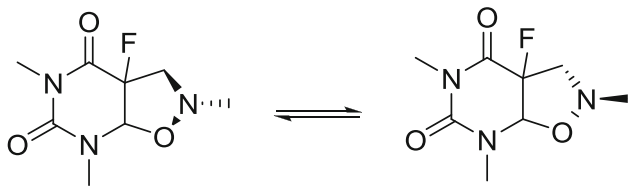

Scheme 3 Nitrogen inversion in C^5-substituted uracil isoxazolidine derivatives

molecule **6a** is expected to exist in two forms **6a–a** and **6a–b**, which differ from each other by both nitrogen configuration and five-membered ring conformation. It becomes clear that to predict the theoretical energy of inversion between those minima, calculations should comply not only nitrogen configuration change, but also ring flip of the isoxazolidine.

We assume that in our model the inversion process begins with low-energy pseudorotation change of structure **6a–a** into the conformer **6a–c**. Relatively slow nitrogen inversion would next transform **6a–c** into the isomer **6a–b**. Pseudorotation of **6a–b** into **6a–d** followed by nitrogen inversion completes the dynamic cycle of the observed process (Fig. 6).

The B3LYP/6-31G(d) geometry optimized structures were used as starting points for other calculations. For brevity, the 6-31 ++G(d,p) basis set was chosen for the DFT (B3LYP, M06 and WB97XD) geometry optimizations of all minima and potential *TS* structures. The comparison of calculated total (H) and relative (ΔE, kcal/mol) energies is shown in Tables 3 and 4.

For accurate and unequivocal determination of the exact conformation of **6a–a**, **6a–b**, **6a–c**, and **6a–d**, a pseudorotation "phase angle" ***P*** and maximum puckering amplitude τ_m were used (Table 5) [44].

Experimental NMR spectra measured in $CDCl_3$ at low temperatures and TFA-*d* do not provide the direct evidence which isomer (**6a–a** or **6a–b**) is preferred. However, both the ^{1}H and ^{13}C chemical shifts show some significant differences for the major and minor forms. The computational chemical shift calculations were performed to find some

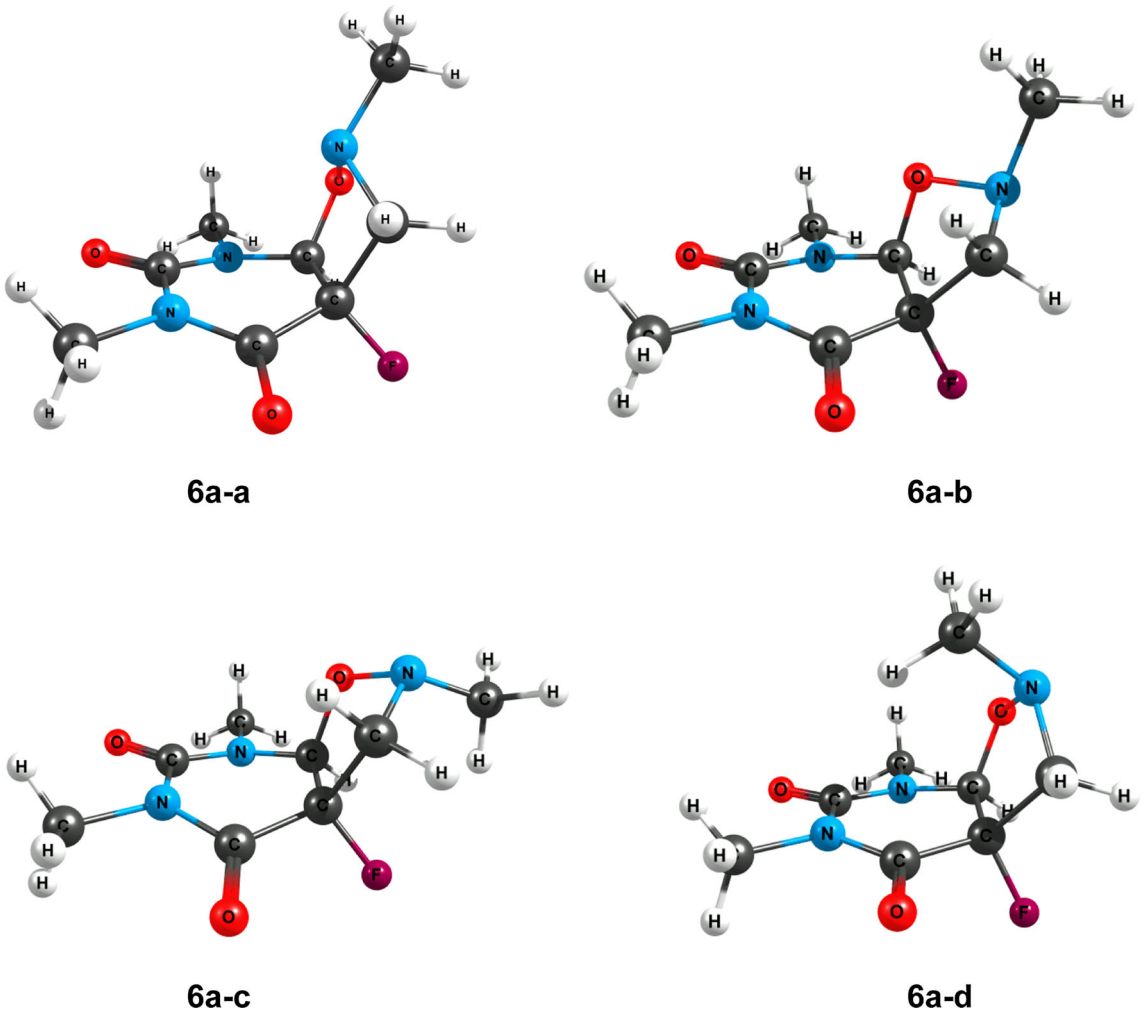

Fig. 5 Results of the DFT B3LYP/6-31++G(d,p) geometry optimizations of four local minima **6a–a**, **6a–b**, **6a–c** and **6a–d**

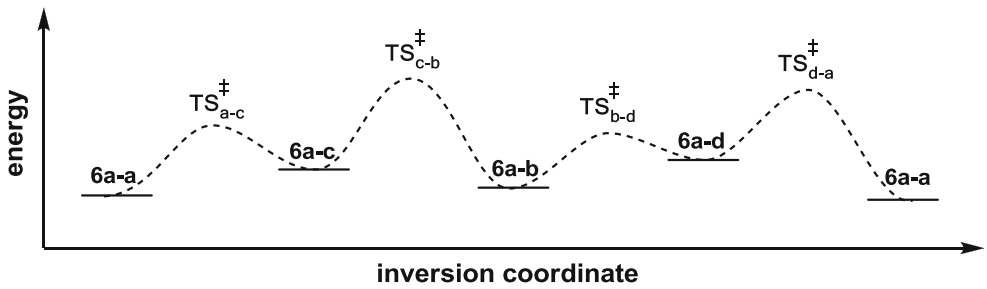

Fig. 6 Nitrogen inversion process in molecule **6a**

relations of these differences to the structural changes. In order to find the most suitable computational model, calculations were carried out using DFT (B3LYP) method with different basis sets: 6–31G(*d*), 6–31G(*d*,*p*), 6–31++G(*d*,*p*), 6–31G(2*d*,2*p*) and 6–31++G(2*d*,2*p*). All the significant relative changes in ^{13}C NMR chemical shifts were reproduced, and DFT GIAO calculations allowed to assign the major form of compound **6a** to the **6a–a** configuration and the minor form of compound **6a** to the **6a–b** configuration (Table 6).

Linear correlation between the chemical shift values of ^{13}C NMR measured experimentally and calculated using B3LYP/6–31++G(2*d*,2*p*) demonstrates a satisfactory assignment of the experimental chemical shift values to the calculated structures of **6a**. An $R^2 = 0.9988$ of major to **6a–a** structure and $R^2 = 0.9992$ of minor to **6a–b**

Table 3 DFT total energies (H), relative energies (ΔE, kcal/mol), activation energies (ΔE_a, kcal/mol) of optimized **6a** structures

	B3LYP//6–31G(*d*)	B3LYP//6–31++G(*d*,*p*)	M06//6–31++G(*d*,*p*)	WB97XD//6–31++G(*d*,*p*)
6a-a[1]	−801.8045	−801.8557	−801.4054	−801.6164
6a-c[1]	−801.8024	−801.8525	−801.4032	−801.6138
6a-b[1]	−801.8038	−801.8562	−801.4053	−801.6160
$TS^1_{a\text{-}c}$	−801.8018	−801.8517	−801.4026	−801.6069
$TS^1_{c\text{-}b}$	−801.7824	−801.8343	−801.3843	−801.5939
$\Delta E^2_{6a\text{-}c–6a\text{-}a}$	1.28	1.99	1.34	1.58
$\Delta E^2_{6a\text{-}c–6a\text{-}b}$	0.86	2.31	1.29	1.33
$\Delta E^3_{a6a\text{-}a–6a\text{-}c}$	1.71	2.52	1.72	5.95
$\Delta E^3_{a6a\text{-}c–6a\text{-}b}$	12.57	11.43	11.89	12.53
$\Delta E_{inv.}$[4]	13.85	13.42	13.23	14.12

[1] Total energies (E^{total}, Hartree) of optimalized structures

[2] Energy differences (ΔE, kcal/mol) between structures

[3] Activation energy (ΔE_a, kcal/mol) calculated as the DFT energy difference ($E^{total}(TS) - E^{total}(GS)$, where TS denotes the adequate transition state and GS denotes the energy of invertomer in its ground state

[4] Total inversion energy ($\Delta E_{inv.}$, kcal/mol) of **6a–a**, >**6a–b** process

Table 4 DFT total energies (H), relative energies (ΔE, kcal/mol), activation energies (ΔE_a, kcal/mol) of optimized **6a** structures

	B3LYP//6–31G(*d*)	B3LYP//6–31++G(*d*,*p*)	M06//6–31++G(*d*,*p*)	WB97XD//6–31++G(*d*,*p*)
6a-b[1]	−801.8038	−801.8562	−801.4053	−801.6159
6a-d[1]	−801.7999	−801.8500	−801.4024	−801.6132
6a-a[1]	−801.8045	−801.8557	−801.4054	−801.6164
$TS^2_{b\text{-}d}$	−801.7995	−801.8501	−801.4007	−801.6116
$TS^2_{d\text{-}a}$	−801.7841	−801.8347	−801.3872	−801.5964
$\Delta E^3_{6a\text{-}d–6a\text{-}b}$	2.43	3.86	1.83	1.71
$\Delta E^3_{6a\text{-}d–6a\text{-}a}$	2.86	3.54	1.88	1.97
$\Delta E^3_{a6a\text{-}b–6a\text{-}d}$	2.68	3.84	2.86	2.75
$\Delta E^3_{a6a\text{-}d–6a\text{-}a}$	9.95	9.66	9.53	10.53
$\Delta E^4_{inv.}$	12.38	13.52	11.36	12.25

[1] Total energies (E^{total}, Hartree) of optimalized structures

[2] Energy differences (ΔE, kcal/mol) between structures

[3] Activation energy (ΔE_a, kcal/mol) calculated as the DFT energy difference ($E^{total}(TS)$-$E^{total}(GS)$, where TS denotes the adequate transition state and GS denotes the energy of invertomer in its ground state

[4] Total inversion energy ($\Delta E_{inv.}$, kcal/mol) of **6a–b**, >**6a–a** process

Table 5 Calculated values of the phase angle of pseudorotation P (deg.) and the amplitude of pucker of **6a** isoxazolidine ring

Structure	P[°]	τ_m	Conformation
6a–a	86	55	$^{N}T_{O}$
6a–b	249	52	$_{N}T^{O}$
6a–c	263	38	$_{N}T^{O}$
6a–d	117	34	$_{CH2}T^{N}$

structure indicate that the regression line perfectly fits the data. Moreover, GIAO B3LYP/6–31++G(2*d*,2*p*)/IEFPCM($CHCl_3$) calculations between relative chemical shifts of **6a–a** and **6a–b** are linearly correlated ($R^2 = 0{,}9667$) with those observed experimentally (Fig. 7).

In general, our theoretical investigation of compound **6a** has shown that nitrogen-hindered configuration change in fused isoxazolidines is not a simple one step process.

Table 6 ^{13}C NMR chemical shifts (δ, ppm) of **6a–a** and **6a–b** ($CDCl_3$, 253 K). The relative chemical shift changes between two invertomers are calculated as $\Delta\delta = I\delta^{major} - \delta^{minor}I$

Carbon	^{13}C NMR exp. chemical shifts (δ, ppm) of **6a** ($CDCl_3$, 253 K)	$\Delta\delta^{exp}$	^{13}C NMR calc. chemical shifts (δ, ppm) of **6a–a** and **6a–b**[1]	$\Delta\delta^{calc}$	^{13}C NMR calc. chemical shifts (δ, ppm) of **6a–a** and **6a–b**[2]	$\Delta\delta^{calc}$	^{13}C NMR calc. chemical shifts (δ, ppm) of **6a–a** and **6a–b**[3]	$\Delta\delta^{calc}$	^{13}C NMR calc. chemical shifts (δ, ppm) of **6a–a** and **6a–b**[4]	$\Delta\delta^{calc}$
C^{4a}	165.40	0.61	160.64	0.35	162.47	0.34	163.85	0.42	166.14	0.77
C^{4b}	164.79		160.29		162.14		163.43		165.37	
C^{2a}	150.56	0.36	143.75	0.03	146.85	0.44	148.99	0.02	150.45	0.01
C^{2b}	150.20		143.78		146.41		149.00		150.44	
C^{6a}	88.45	0.31	90.86	0.14	93.09	0.84	91.70	0.29	92.25	0.42
C^{6b}	88.76		91.00		92.25		91.41		91.84	
C^{5a}	97.12	1.42	100.21	2.12	101.33	1.74	99.16	1.95	100.72	1.70
C^{5b}	95.70		98.09		99.59		97.20		99.02	
N^{3a}-CH_3	28.59	0.19	29.57	0.79	30.33	0.69	29.64	0.74	30.35	0.55
N^{3b}-CH_3	28.40		28.78		29.64		28.91		29.79	
N^{1a}-CH_3	32.44	2.31	33.43	2.30	35.07	2.13	34.25	2.23	34.70	2.47
N^{1b}-CH_3	34.75		35.74		37.20		36.48		37.17	
C^{9a}	67.80	0.66	70.16	0.96	71.67	1.40	70.50	1.19	70.64	1.17
C^{9b}	67.14		69.21		70.27		69.31		69.47	
N^{8a}-CH_3	44.49	0.38	42.69	0.65	43.60	0.69	43.08	0.65	43.32	0.66
N^{8b}-CH_3	44.87		43.34		44.29		43.74		43.98	

[1] DFT GIAO B3LYP/6–31G(*d*,*p*), geometries from B3LYP/6–31G(*d*,*p*)

[2] DFT GIAO B3LYP/6–31++G(*d*,*p*), geometries from B3LYP/6–31++G(*d*,*p*)

[3] DFT GIAO B3LYP/6–31++G(2*d*,2*p*), geometries from B3LYP/6–31++G(2*d*,2*p*)

[4] DFT GIAO B3LYP/6–31++G(2*d*,2*p*)/IEFPCM($CHCl_3$), geometries from B3LYP/6–31++G(2*d*,2*p*)/IEFPCM($CHCl_3$)

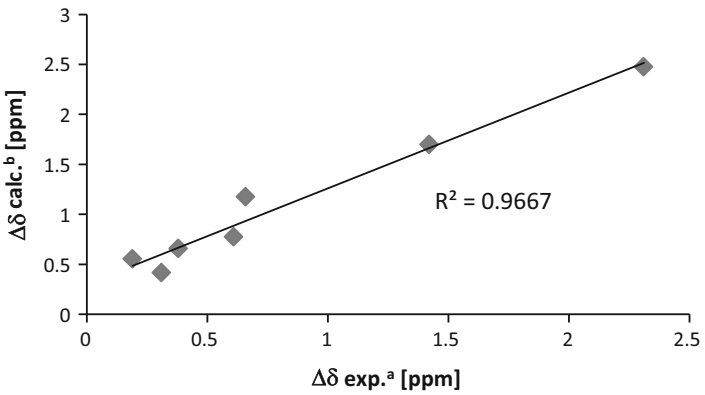

Fig. 7 Relation between the experimental and theoretical (B3LYP/6–31++G(2*d*,2*p*)/IEFPCM($CHCl_3$)) major–minor invertomer shift differences

[a] Δδ exp. calculated as $I\delta^{6a\ major} - \delta^{6a\ minor}I$

[b] Δδ calc. calculated as $I\delta^{6a\text{-}a} - \delta^{6a\text{-}b}I$

Correlation between Δδ exp. = $IC^{2a} - C^{2b}I$ and Δδ calc. = $IC^{2a} - C^{2b}I$ was omitted due to larger error

Moreover, the proper inversion of nitrogen atom is possible only after reaching one of the molecules geometry that has this same configuration of nitrogen but the opposite conformation of the ring compared to starting geometry. According to the B3LYP calculations performed with 6–31++G(*d*,*p*) basis set, the energy barrier for the nitrogen inversion as a total **6a–a** to **6a–b** inversion process is approximately 13.5 kcal/mol. The value of 13.2–13.4 kcal/mol has been reported for similar fused isoxazolidinyl systems [36]. DFT GIAO calculations demonstrate compliance of experimental and calculated chemical shift values for major and minor invertomer of compound **6a**.

Conclusions

In this study, we have synthesized fused isoxazolidines via an intramolecular 1,3-dipolar cycloaddition of various *N*-alkyl methylenenitrones with 5-substituted uracil derivatives. The cycloadducts were characterized by spectroscopic and structural techniques as well as the theoretical methods. These reactions proceed with complete diastereoselectivity and regioselectivity. The obtained isoxazolidines exist as equilibrating mixtures of invertomers due to slow nitrogen inversion. The NMR studies on the conformation of invertomers and on the inversion rates showed the effect of *N*-alkyl substituents and C^5-substituents both on the geometry of the ring and on the inversion barrier. The nitrogen inversion barrier for **6a** was determined using DFT quantochemical calculations and was found to be 13,5 kcal/mol. The experimental and theoretical ^{13}C NMR chemical shifts are in good agreement with each other. In addition, the theoretical relative chemical shifts of **6a–a** and **6a–b** showed very good correlation with the experimental data. Further theoretical investigation on nitrogen inversion of the title compounds is currently under way.

References

1. Kore AM, Charles I (2012) Curr Org Chem 16:1996–2013
2. Boncel S, Gondela A, Walczak K (2008) Curr Org Synth 5:365–396
3. Padwa A, Pearson WH (2002) Synthetic applications of 1,3-dipolar cycloaddition chemistry toward heterocycles and natural products. Wiley, New York
4. Pellissier H (2007) Tetrahedron 63:3235–3285
5. Nishiwaki N (2014) Methods and applications of cycloaddition reactions in organic synthesis. Wiley, Hoboken
6. Keana JFW, Mason FP, Bland JS (1969) J Org Chem 34:3705–3707
7. Saladino R, Stasi L, Crestini C, Nicoletti R, Botta M (1997) Tetrahedron 53:7045–7056
8. Pellissier H, Rodriguez J, Vollhardt KPC (1999) Chem Eur J 5:3549–3561
9. Negrón G, Calderón G, Vazquez F, Lomas L, Cardenas J, Marquez C, Gavino R (2002) Synth Commun 32:1977–1984
10. Colacino E, De Luca G, Liguori A, Napoli A, Siciliano C, Sindona G (2003) Nucleosides Nucleotides Nucleic Acids 22:743–745
11. Bloch R (1998) Chem Rev 98:1407–1438
12. Gothelf KV, Jørgensen KA (1998) Chem Rev 98:863–909
13. Villamena FA, Xia S, Merle JK, Lauricella R, Tuccio B, Hadad CM, Zweier JL (2007) J Am Chem Soc 129:8177–8191
14. Slemmer JE, Shacka JJ, Sweeney MI, Weber JT (2008) Curr Med Chem 15:404–414
15. Dias AG, Santos CEV, Cyrino FZGA, Bouskela E, Costa PRR (2009) Bioorgan Med Chem 17:3995–3998
16. Feuer H, Torssell K (2008) Nitrile oxides, nitrones and nitronates in organic synthesis. Novel strategies in synthesis. Wiley, Hoboken
17. Chiacchio U, Padwa A, Romeo G (2009) Curr Org Chem 13:422–447
18. Legon AC (1980) Chem Rev 80:231–262
19. Raban M, Kost D (1984) Tetrahedron 40:3345–3381
20. Ali SA, Hassan A, Wazeer MIM (1995) Spectrochim Acta A M 51:2279–2287
21. Ali SA, Iman MZN, Wazeer MIM, Fettouhi MB (2008) Spectrochim Acta A M 70:482–490
22. Borch RF, Bernstein MD, Durst HD (1971) J Am Chem Soc 93:2897–2904
23. West RA, Barrett HW (1954) J Am Chem Soc 76:3146–3148
24. Zajac MA, Zakrzewski AG, Kowal MG, Narayan S (2003) Synth Commun 33:3291–3297
25. Rabinowitz JL, Gurin S (1953) J Am Chem Soc 75:5758–5759
26. Gaussian 09 Revision D.01, Frisch MJ, Trucks GW, Schlegel HB, Scuseria GE, Robb MA, Cheeseman JR, Scalmani Barone GV, Mennucci B, Petersson GA, Nakatsuji H, Caricato M, Li X, Hratchian HP, Izmaylov AF, Bloino J, Zheng G, Sonnenberg JL, Hada M, Ehara M, Toyota K, Fukuda R, Hasegawa J, Ishida M, Nakajima T, Honda Y, Kitao O, Nakai H, Vreven T, Montgomery JA Jr, Peralta JE, Ogliaro F, Bearpark M, Heyd JJ, Brothers E, Kudin KN, Staroverov VN, Keith T, Kobayashi R, Normand J, Raghavachari K, Rendell A, Burant JC, Iyengar SS, Tomasi J, Cossi M, Rega N, Millam JM, Klene M, Knox JE, Cross JB, Bakken V, Adamo C, Jaramillo J, Gomperts R, Stratmann RE, Yazyev O, Austin AJ, Cammi R, Pomelli C, Ochterski JW, Martin RL, Morokuma K, Zakrzewski VG, Voth GA, Salvador P, Dannenberg JJ, Dapprich S, Daniels AD, Farkas O, Foresman JB, Ortiz JV, Cioslowski J, Fox DJ (2013) Gaussian Inc Wallingford CT
27. Becke AD (1988) Phys Rev A 38:3098–3100
28. Chai JD, Head-Gordon M (2008) Phys Chem Chem Phys 44:6615–6620
29. Zhao Y, Truhlar DG (2008) Theor Chem Acc 120:215–241
30. Cances E, Mennucci B (1998) J Math Chem 23:309–326
31. Ditchfield R (1972) J Chem Phys 56:5688–5691
32. Wójtowicz-Rajchel H, Koroniak H, Katrusiak A (2008) Eur J Org Chem 2008:368–376
33. Wójtowicz-Rajchel H, Pasikowska M, Olejniczak A, Kartusiak A, Koroniak H (2010) New J Chem 34:894–902
34. Wójtowicz-Rajchel H, Koroniak H (2012) J Fluorine Chem 135:225–230

35. Raban M, Jones FB, Carlson EH, Banucci E, LeBel NA (1970) J Org Chem 35:1496–1499 **(and references cited therein)**
36. Hassner A, Maurya R, Friedman O, Gottlieb HE, Padwa A, Austin D (1993) J Org Chem 58:4539–4546
37. Nenajdenko VG, Sanin AV, Tok OL, Balenkova ES (1999) Chem Heterocycl Compd 35:348–357
38. Huisgen R (1984) 1,3-Dipolar Cycloaddition. Introduction, Survey, Mechanics In 1,3-Dipolar Cycloaddition Chemistry, vol 1. Wiley-Interscience, New York, pp 1–176
39. Undheim K, Benneche T (1996) Pyrimidines and Their Benzo Derivatives. In: Katritzky AR, Rees CW, Scriven EF (eds) Comprehensive Heterocyclic Chemistry VI, (5th edn). Pergamon, Pergamon
40. Shishkin OV, Gorb L, Leszczynski J (2000) Int J Mol Sci 1:17–27
41. Roberts JD (1959) Nuclear magnetic resonanse. Applications to organic chemistry. McGraw-Hill Book Company, New York
42. Eliel EL, Wilen SH, Mander LN (1994) Stereochemistry of organic compounds. Wiley, New York
43. DeShong P, Dicken CM, Staib RR, Freyer AJ, Weinreb SM (1982) J Org Chem 47:4397–4403
44. Altona C, Sundaralingam M (1972) J Am Chem Soc 94:8205–8212